J Membrane Biol (2010) 236:27–36
DOI 10.1007/s00232-010-9277-y

Life Cycle of an Electropore: Field-Dependent and Field-Independent Steps in Pore Creation and Annihilation

Zachary A. Levine · P. Thomas Vernier

Received: 5 January 2010 / Accepted: 11 June 2010 / Published online: 11 July 2010

Abstract Electropermeabilization, an electric field-induced modification of the barrier functions of the cell membrane, is widely used in laboratories and increasingly in the clinic; but the mechanisms and physical structures associated with the electromanipulation of membrane permeability have not been definitively characterized. Indirect experimental observations of electrical conductance and small molecule transport as well as molecular dynamics simulations have led to models in which hydrophilic pores form in phospholipid bilayers with increased probability in the presence of an electric field. Presently available methods do not permit the direct, nanoscale examination of electroporated membranes that would confirm the existence of these structures. To facilitate the reconciliation of poration models with the observed properties of electropermeabilized lipid bilayers and cell membranes, we propose a scheme for characterizing the stages of electropore formation and resealing. This electropore life cycle, based on molecular dynamics simulations of phospholipid bilayers, defines a sequence of discrete steps in the electric field-driven restructuring of the membrane that leads to the formation of a head group-lined, aqueous pore and then, after the field is removed, to the dismantling of the pore and reassembly of the intact bilayer. Utilizing this scheme we can systematically analyze the interactions between the electric field and the bilayer components involved in pore initiation, construction and resealing. We find that the pore creation time depends strongly on the electric field gradient across the membrane interface and that the pore annihilation time is at least weakly dependent on the magnitude of the pore-initiating electric field and, in general, much longer than the pore creation time.

Keywords Electropermeabilization · Electroporation · Molecular dynamics · Pore life cycle · Pore creation · Pore annihilation

Z. A. Levine · P. T. Vernier (✉)
MOSIS, Information Sciences Institute, Viterbi School of Engineering, University of Southern California, 4676 Admiralty Way, Marina del Rey, CA 90292, USA
e-mail: vernier@mosis.com

Z. A. Levine
Department of Physics and Astronomy, University of Southern California, Los Angeles, CA, USA
e-mail: zlevine@mosis.com

P. T. Vernier
Ming Hsieh Department of Electrical Engineering, Viterbi School of Engineering, University of Southern California, Los Angeles, CA, USA

Introduction

The structural integrity of the cell membrane, essential for compartmentalization of extracellular and intracellular materials, can be disrupted with electrically induced permeabilization (electroporation) (Hamilton and Sale 1967; Rols and Teissie 1990), which results in increased electrical conductance and the influx and efflux of normally impermeant small and large molecules (Neumann et al. 1982; Rols et al. 1992; Mir et al. 1999). Small changes in conductance can be measured within a few nanoseconds after the application of a pulsed electric field (Benz and Zimmermann 1980), and fluorescent dyes can be used as molecular markers to indicate the degree of membrane permeabilization; but the detailed mechanisms of electropermeabilization are difficult to access experimentally (Teissie et al. 2005), even with nanoscale instrumentation

such as atomic force microscopy (AFM). Other analytical methods, including continuum and atomic-level molecular simulations, provide windows for investigating electropore formation at the nanoscale, where there are at present no direct observational tools.

In molecular dynamics (MD) simulations of electroporation (Tieleman et al. 2003; Tarek 2005) the electric field-driven formation of a water column across the bilayer interior is followed by the construction of a bridge of hydrophilic lipid head groups and additional hydrating water molecules. Although it has been shown that the pore creation time decreases as the pore-initiating electric field increases (Ziegler and Vernier 2008), the detailed time course of electropore construction and annihilation in MD simulations has not been quantitatively characterized, though several pioneering studies have described the key steps in the electroporation process (Tieleman et al. 2003; Tieleman 2004; Tarek 2005). Here, we propose a scheme for objectively classifying and delineating the stages in the life cycle of an electropore.

The establishment of objective criteria for analyzing the appearance and disappearance of membrane pores in electric fields permits quantifying and tying more closely to molecular mechanisms the dependence of poration-associated processes on the electric field strength and other variables and facilitates comparisons of electropermeabilization in different model systems. Because electroporation is strongly dependent on the interactions between interface water molecules and lipid head groups (Tieleman 2004; Tarek 2005; Ziegler and Vernier 2008), even small differences in force fields and other simulation parameters may be expected to produce significant differences in electropore creation and annihilation dynamics. Examples are provided.

Materials and Methods

Simulation Conditions

All simulations were performed using the GROMACS set of programs, version 3.3.3 (Van der Spoel et al. 2005), on the University of Southern California High Performance Computing and Communications Linux cluster (http://www.usc.edu/hpcc/). Lipid topologies were derived from OPLS united-atom parameters (Berger et al. 1997) and obtained from Peter Tieleman of the University of Calgary (http://moose.bio.ucalgary.ca). The simple point charge (SPC) water model was used (Berendsen et al. 1981). Systems were coupled to a temperature bath at 310 K with a relaxation time of 0.1 ps and a pressure bath at 1 bar with a relaxation time of 1 ps, each using a weak coupling algorithm (Berendsen et al. 1984). Pressure was coupled semi-isotropically (using a compressibility of 4.5×10^{-5} bar^{-1}) normal to and in the plane of the membrane. Bond lengths were constrained using the LINCS algorithm (Hess et al. 1997) for lipids and SETTLE (Miyamoto and Kollman 1992) for water. Short-range electrostatic and Lennard-Jones interactions were cut off at 1.0 nm. Long-range electrostatics were calculated by the PME algorithm (Essmann et al. 1995) using fast Fourier transforms and conductive boundary conditions. Reciprocal-space interactions were evaluated on a 0.12-nm grid with fourth-order B-spline interpolation. The parameter ewald_rtol, which controls the relative error for the Ewald sum in the direct and reciprocal space, was set to 10^{-5}. Periodic boundary conditions were employed to mitigate system size effects.

Systems and Structures

All systems contained 128 lipid molecules—1-palmitoyl-2-oleoyl-*sn*-glycero-3-phosphatidylcholine (POPC) or 1,2-dioleoyl-*sn*-glycero-3-phosphatidylcholine (DOPC)—and at least 4,480 water molecules (~35 waters/lipid), which resulted in a system box size of approximately $7 \times 7 \times 7$ nm. POPC systems used for tracking the complete life cycle, both pore creation and annihilation, contained more water (~70 waters per lipid) and thus were about 10 nm in the z dimension. Simulations with multiple trials were run in parallel, starting from the same initial positions. To ensure that each trial was independent, every atom was assigned a randomized velocity from a Maxwell distribution at the beginning of the simulation (a built-in function of GROMACS). All systems were equilibrated until they attained a constant area per lipid: POPC 0.66 nm^2, DOPC 0.65 nm^2, second DOPC model (see below) 0.67 nm^2. Pore creation times were measured at four external electric fields—300, 400, 500 and 600 MV/m—with three independent trials at each electric field strength (300 MV/m in vacuum corresponds to an effective electric field in aqueous medium of about 4 MV/m). POPC pore annihilation times were taken from a separate set of simulations in which the pore-initiating external electric fields were 320, 400 and 600 MV/m. At least three trials per field were used for annihilation times. We tested two DOPC models, an older version, which was obtained from Peter Tieleman in 2005 (personal communication), and a newer version, currently available at http://moose.bio.ucalgary.ca/. We refer to these as DOPC (2005) and DOPC (2009), respectively. These models differ slightly in the charge distribution for the atoms in the head group and glycerol backbone.

Electropore Life Cycle

We divide the electropore life cycle broadly into pore creation and pore annihilation. Pore creation is comprised

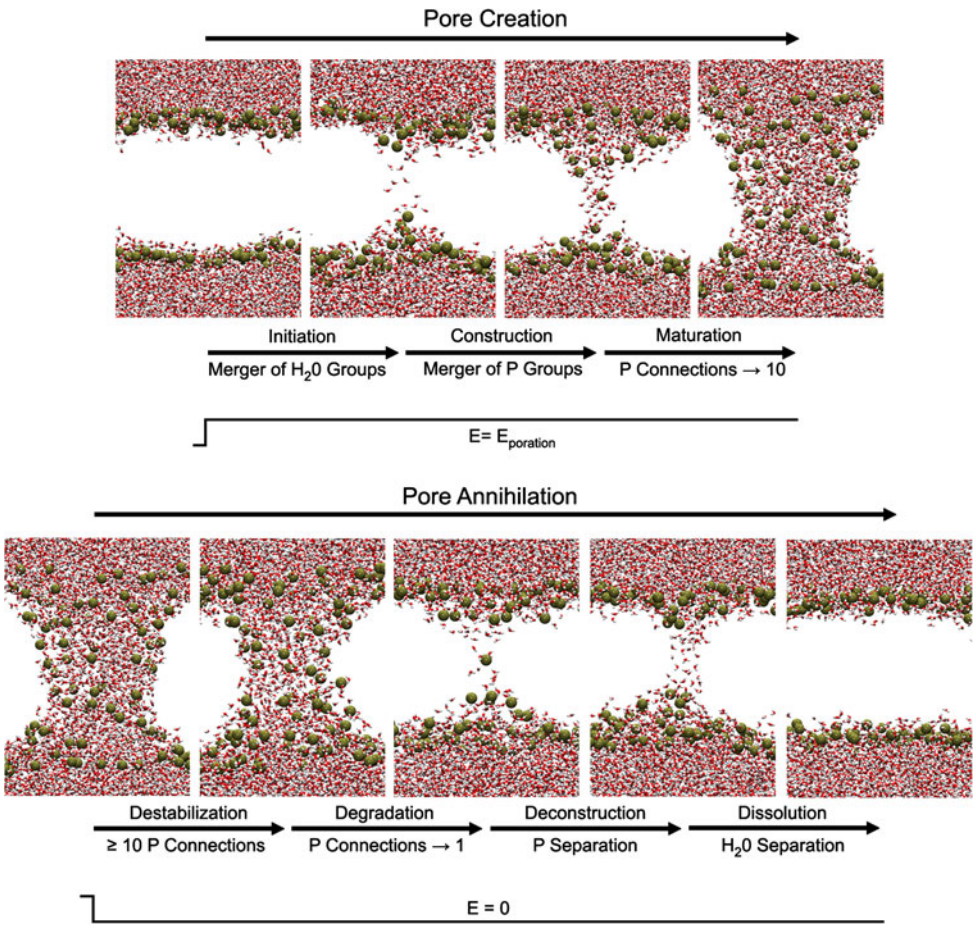

Fig. 1 Life cycle of an electropore. Only water and phosphorus atoms are shown for simplicity. Pore creation in an electric field begins with the introduction of a water defect into the bilayer interior (pore initiation), followed by the reorganization of phospholipid head groups in each leaflet around the defect (pore construction). Migration of additional water and head groups into the pore continues until an arbitrarily defined mature pore structure is formed (pore maturation). Pore annihilation begins with the removal of the porating electric field. The pore structure is quasi-stable at this time (pore destabilization), but soon there is a decrease in pore size as head groups and water begin to migrate out of the membrane interior (pore degradation). The head groups separate again into two groups (pore deconstruction). Water quickly follows (pore dissolution), and the intact structure of the bilayer is restored

of three stages: initiation, construction and maturation (defined below). Pore annihilation begins when the external electric field is removed from a mature pore structure and proceeds through destabilization, degradation, deconstruction and dissolution (Fig. 1).

Pore Creation

Pore initiation begins with the application of an external electric field and ends when the two groups of water molecules, initially separated by the bilayer, merge to become a single group (nonzero water density in every 100-pm slice between the two mean planes of phosphorus atoms). In some simulations the combined water groups split again, in less than 400 ps after the joining in each case. These transient events were not counted as mergers. Pore construction begins with the formation of the membrane-spanning water column (hydrophobic pore [Abidor et al. 1979]) that marks the merger of the water groups and ends when the phosphorus groups that are initially found on the two leaflets of the bilayer follow the water into the membrane interior and merge into a single phosphorus group. A group is defined as a set of atoms, each separated by a maximum distance of 1.2 nm (Sengupta et al. 2008). Because water and the charged phospholipid head groups now bridge the membrane interior, this structure is comparable to what has been called in several contexts a hydrophilic pore (Weaver and Mintzer 1981; Glaser et al. 1988; Leontiadou et al. 2004). Continued application of the porating electric field results in an evolution, or maturation, of the hydrophilic pore. We define a mature pore arbitrarily as a hydrophilic pore in which at least 10 phosphorus atoms from the initial anodic leaflet are found within 1.2 nm of phosphorus atoms from the cathodic leaflet.

Pore Annihilation

Pore destabilization, the first stage of pore annihilation, is the quasi-stable period after the field is removed during which the number of anode to cathode phosphorus connections fluctuates around the mature pore criterion (10 connections). Pore degradation begins when the number of anode to cathode phosphorus connections drops below 10 and ends when there is only one anode to cathode phosphorus connection (Fig. 2). The pore diameter decreases during this time to a minimum, about 0.4–0.6 nm. Pore deconstruction, another quasi-stable period, terminates

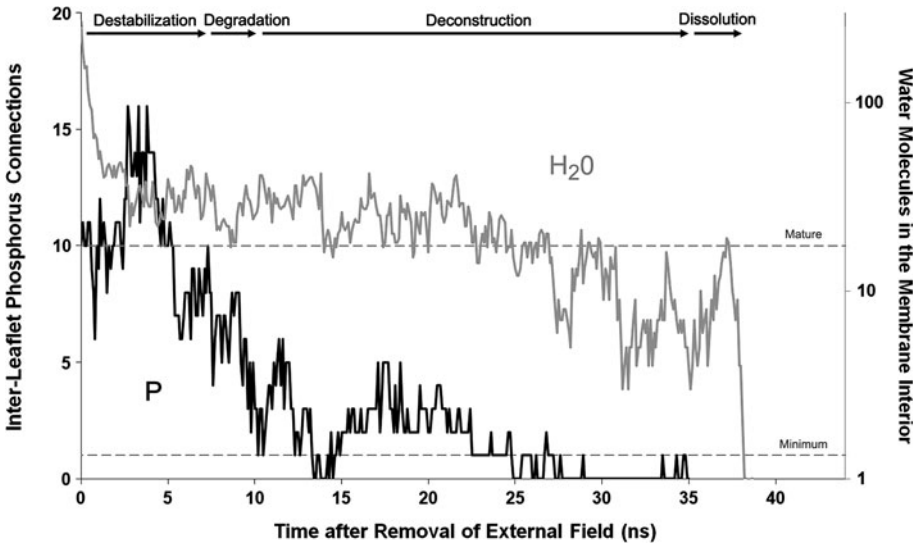

Fig. 2 Phosphorus and water distribution during pore annihilation. The number of interleaflet phosphorus connections (anodic phosphorus atoms located within 1.2 nm of cathodic phosphorus atoms) remains relatively constant for some time (destabilization stage) after the external electric field is removed from a system containing a mature pore, even though a significant amount of water leaves the pore during this period. During pore degradation the number of phosphorus connections falls from 10 to one. Pore deconstruction ends when all phosphorus connections have been broken. Pore dissolution, the final step in pore annihilation, terminates when water is no longer present in the bilayer interior

when the single phosphorus group of the porated bilayer splits into two groups, which remain separate for the remainder of the simulation. At the end of pore deconstruction only the water column remains. We call the disassembly of the water column pore dissolution.

Individual pore life cycle times were calculated using a custom Perl program, which codifies the stage boundaries described above. The local electric field profile was extracted using the GROMACS function "g potential," which integrates the charge density found in bins (0.1 nm in width) parallel to the plane of the bilayer. Charges are rearranged due to the application of a user-defined external electric field, which is constant throughout the system. Figure 3 shows a typical electric field profile for a POPC bilayer with an external field of 300 MV/m. The average value of the local electric field within 0.5 nm of the bilayer mid-plane is referred to here as the "membrane internal electric field" and was calculated from the electric field profile averaged from 100 ps after the external field was applied to 200 ps before pore construction began. Because the net electric field in bulk water is much smaller than the field in the membrane interior (as a consequence of the high permittivity of water and the low permittivity of the phospholipid hydrocarbon tails), the magnitude of the membrane internal electric field may be regarded as essentially equivalent to the electric field gradient across the membrane interface. Additionally, we calculated the "box potential" in each system by multiplying the applied electric field by the box length in the direction of the electric field ($E \cdot L_z$). This value is comparable to the

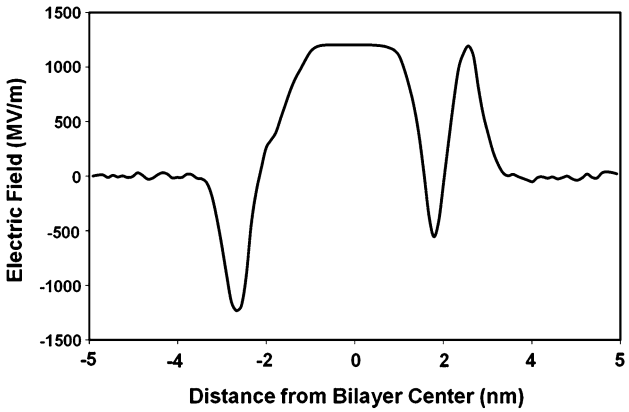

Fig. 3 Electric field profile for a POPC bilayer. When an external electric field is applied to a POPC bilayer, the local electric field can be calculated by integrating the charge density in discrete planes (parallel to the plane of the bilayer and 0.1 nm in width). This value is determined by the rearrangement of charge in the system. The membrane internal electric field is calculated by averaging the local electric field at the bilayer mid-plane (±0.5 nm) from 100 ps after the external electric field is applied to 200 ps before pore construction begins

transmembrane potential reported in other work (Tieleman 2004; Tarek 2005), where the membrane thickness is a large fraction of the box length.

Images

Molecular graphics images were generated with visual molecular dynamics (VMD) (Humphrey et al. 1996).

Results

Pore Creation and Annihilation—POPC

As models (Weaver and Chizmadzhev 1996) and intuition predict, the pore creation time for POPC bilayers decreases with increasing electric fields (Table 1). This is almost entirely a result of the time required for pore initiation, the first stage of pore creation. Pore construction time and pore maturation time (an end point defined somewhat arbitrarily for this initial study) are only slightly dependent on the electric field strength.

Pore annihilation times are significantly longer than pore creation times (Table 2). In pore creation, once the initial membrane-spanning water column is formed, it takes less than 1 ns for the head groups to follow the water into the bilayer interior. When the electric field is removed, however, tens of nanoseconds elapse before the head groups migrate back to the bilayer leaflets. During pore destabilization, the period immediately following removal of the electric field, the number of water molecules in the pore (within 0.5 nm of the bilayer mid-plane) decreases substantially in about a nanosecond and the pore diameter decreases to about 0.6 nm. In a small percentage of cases pore annihilation continues to the next stage with no delay, but usually the pore remains intact, with the number of interleaflet phosphorus connections fluctuating around 10, for a time that ranges from less than 1 to over 20 ns (Fig. 2). At some point (the end of the destabilization stage) the number of anode to cathode phosphorus atom connections permanently declines from 10 or more to one—the reverse evolution of the developed pore to a

Table 1 POPC pore creation times

Applied field (MV/m)	Box potential (V)	Average internal field (MV/m)	Initiation		Construction		Maturation		Creation	
			Time (ns)	Mean (ns)	Time (ns)	Mean (ns)	Time (ns)	Mean (ns)	Time (ns)	Mean (ns)
			11.2		0.2		0.8		12.2	
300	3.2	1,253	10.0	9.5 ± 2.0	0.2	0.3 ± 0.1	0.4	0.6 ± 0.2	10.6	10.4 ± 1.9
			7.3		0.4		0.7		8.4	
			2.8		0.0		0.5		3.3	
400	4.2	1,630	2.3	2.0 ± 1.0	0.3	0.2 ± 0.2	1.1	0.8 ± 0.3	3.7	2.9 ± 1.1
			0.8		0.2		0.7		1.7	
			0.9		0.1		1.0		2.0	
500	5.3	2,180	0.6	0.6 ± 0.3	0.2	0.2 ± 0.1	0.5	0.8 ± 0.3	1.3	1.6 ± 0.4
			0.4		0.3		0.9		1.6	
			0.5		0.1		0.1		0.7	
600	6.3	2,347	0.5	0.4 ± 0.2	0.0	0.1 ± 0.1	0.3	0.2 ± 0.1	0.8	0.7 ± 0.1
			0.2		0.2		0.2		0.6	

Table 2 POPC pore annihilation times

Applied field (MV/m)	Destabilization		Degradation		Deconstruction		Dissolution		Annihilation	
	Time (ns)	Mean (ns)	Time (ns)	Mean (ns)	Time (ns)	Mean (ns)	Time (ns)	Mean (ns)	Time (ns)	Mean (ns)
	0.1		0.6		31.1		0.8		32.6	
320	4.7	12.9 ± 12.4	6.8	5.3 ± 5.0	37.7	27.6 ± 11.2	2.9	1.3 ± 1.1	52.1	47.1 ± 15.9
	21.6		2.1		11.5		1.1		36.3	
	25.2		11.6		30.0		0.4		67.2	
	7.3		3.0		24.6		2.9		37.8	
400	15.5	13.0 ± 12.5	1.0	2.2 ± 1.3	7.7	18.5 ± 8.5	2.5	1.9 ± 1.0	26.7	35.6 ± 18.1
	29.2		3.7		25.9		1.1		59.9	
	0.1		1.2		15.6		1.0		17.9	
	11.4		1.0		8.1		1.5		22.0	
600	3.8	5.2 ± 5.7	6.4	3.4 ± 2.7	28.5	26.6 ± 17.6	0.7	0.9 ± 0.5	39.4	36.1 ± 12.8
	0.3		2.9		43.1		0.6		46.9	

minimum, single phosphorus group structure. The time required for this decline, the pore degradation time, is typically several nanoseconds, significantly longer than pore maturation, the corresponding pore creation stage. Destabilization and degradation times have large standard deviations, indicating the stochastic nature of the processes underlying these stages of pore annihilation. At the highest porating field, however, there is a significant reduction in the destabilization time, suggesting that pore destabilization has a field-dependent component. Pore deconstruction (separation into two phosphorus groups) and dissolution (expulsion of water from the membrane interior) are apparently independent of field strength. Deconstruction times are tens of nanoseconds, with large standard deviations; the minimal hydrophilic pore is quasi-stable. Pore dissolution, on the other hand, is rapid; the hydrophobic pore is highly unstable.

Pore Creation—POPC Versus DOPC

POPC and DOPC bilayers have similar minimum porating electric fields (Ziegler and Vernier 2008), so we might expect similarities in their electropore life cycles. Here, we report individual pore creation stage times for DOPC (2005) and DOPC (2009) bilayers (Tables 3, 4) and compare these patterns with those found for POPC (Table 5). To simplify the comparisons, the POPC simulations were carried out with the same system size as the DOPC simulations. DOPC pore initiation is strongly field-dependent, similar to POPC. DOPC pore construction and maturation

Table 3 DOPC (2005) pore creation times

Applied field (MV/m)	Box potential (V)	Average internal field (MV/m)	Initiation		Construction		Maturation		Creation	
			Time (ns)	Mean (ns)	Time (ns)	Mean (ns)	Time (ns)	Mean (ns)	Time (ns)	Mean (ns)
			>25		N/A		N/A		>25	
300	2.2	820	>25	N/A	N/A	N/A	N/A	N/A	>25	>25
			>25		N/A		N/A		>25	
			>25		N/A		N/A		>25	
400	3.0	1,100	21.3	>15.4 ± 8.3	0.2	0.2 ± 0.0	0.8	0.7 ± 0.1	22.3	>16.3 ± 8.5
			9.5		0.2		0.6		10.3	
			6.1		0.3		0.4		6.8	
500	3.7	1,333	4.6	3.9 ± 2.6	0.1	0.2 ± 0.1	0.3	0.4 ± 0.1	5.0	4.5 ± 2.6
			1.0		0.2		0.5		1.7	
			1.4		0.1		0.2		1.7	
600	4.4	1,747	1.3	1.1 ± 0.5	0.1	0.2 ± 0.1	0.3	0.2 ± 0.1	1.7	1.5 ± 0.4
			0.5		0.3		0.2		1.0	

Table 4 DOPC (2009) pore creation times

Applied field (MV/m)	Box potential (V)	Average internal field (MV/m)	Initiation		Construction		Maturation		Creation	
			Time (ns)	Mean (ns)	Time (ns)	Mean (ns)	Time (ns)	Mean (ns)	Time (ns)	Mean (ns)
			>25		N/A		N/A		>25	
300	2.1	793	>25	N/A	N/A	N/A	N/A	N/A	>25	N/A
			>25		N/A		N/A		>25	
			>25		N/A		N/A		>25	
400	2.9	1147	15.6	>14.8 ± 1.2	0.2	0.3 ± 0.1	0.7	0.5 ± 0.2	16.5	>15.6 ± 1.3
			13.9		0.4		0.4		14.7	
			7.0		0.2		0.3		7.5	
500	3.6	1437	1.6	3.1 ± 3.4	0.1	0.2 ± 0.1	0.5	0.4 ± 0.1	2.2	3.7 ± 3.3
			0.8		0.3		0.4		1.5	
			2.4		0.1		0.3		2.8	
600	4.3	1837	1.6	1.8 ± 0.6	0.1	0.1 ± 0.1	0.2	0.3 ± 0.1	1.9	2.2 ± 0.6
			1.3		0.2		0.3		1.8	

Table 5 POPC pore creation times

Applied field (MV/m)	Box potential (V)	Average internal field (MV/m)	Initiation		Construction		Maturation		Creation	
			Time (ns)	Mean (ns)	Time (ns)	Mean (ns)	Time (ns)	Mean (ns)	Time (ns)	Mean (ns)
			>25		>25		>25		>25	
300	2.1	861	>25	>25	>25	>25	>25	>25	>25	>25
			>25		>25		>25		>25	
			15.2		0.3		0.5		16.0	
400	2.9	1,090	12.8	11.2 ± 5.1	0.1	0.1 ± 0.2	0.6	0.5 ± 0.1	13.5	11.8 ± 5.3
			5.5		0.0		0.4		5.9	
			4.8		0.0		0.3		5.1	
500	3.6	1,420	3.3	2.9 ± 2.1	0.2	0.1 ± 0.1	0.3	0.4 ± 0.2	3.8	3.4 ± 2.0
			0.6		0.0		0.6		1.2	
			1.8		0.3		0.4		2.5	
600	4.3	1,783	1.2	1.3 ± 0.5	0.1	0.2 ± 0.1	0.2	0.3 ± 0.1	1.5	1.8 ± 0.6
			0.9		0.1		0.3		1.3	

System geometry similar to the DOPC (2005) and DOPC (2009) systems, as described in Materials and Methods

times, like those for POPC, exhibit only a small dependence on electric field strength. Each of the DOPC stage times is comparable to the corresponding POPC time. All three systems appear to have a smaller variance in pore creation time as the strength of the external electric field is increased, implying that stochastic effects are less dominant at higher fields.

Pore creation times in all three systems are inversely dependent on the magnitude of the bilayer internal electric field (Fig. 4). Membrane internal electric fields (and thus the field gradient across the interface) in DOPC and POPC systems of the same size are similar (Tables 3, 4, 5). In the POPC simulations with a longer box z dimension (Table 1) the membrane internal electric field for a given external field is higher, a consequence of how the external electric field is implemented in Gromacs (Gurtovenko and Vattulainen 2009).

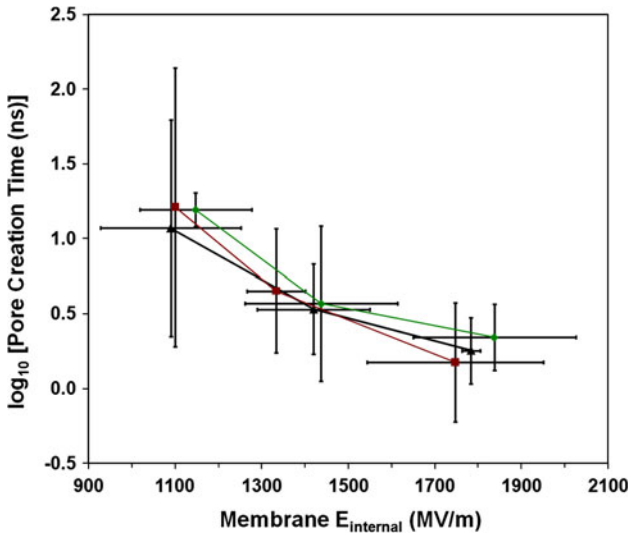

Fig. 4 Log (pore creation time) vs. membrane internal electric field for POPC (*filled triangle*), DOPC (2005) (*filled square*) and DOPC (2009) (*filled diamond*). *Error bars* (1 SD) are shown for both the internal electric field values and pore creation times. Values for POPC were taken from Table 5. These systems have dimensions comparable to those in the DOPC systems

Pore Creation—DOPC (2005) Versus DOPC (2009)

Even though DOPC (2005) and DOPC (2009) have somewhat different charge distributions, the differences in the electric field profile across the membrane interface for these two systems do not appreciably affect electropore creation dynamics. Pore creation times (and the times for the initiation, construction and maturation stages) are similar, as shown in Tables 3 and 4 and in Fig. 4. The common feature in the two DOPC systems (and the corresponding POPC system) is the magnitude of the electric field in the membrane interior and the resulting net gradient across the interface.

Discussion

We have presented a scheme for dividing the electroporation of lipid bilayers, as represented in MD simulations, into discrete stages, using the evolving distributions of water and phospholipid head groups (phosphorus atoms) as indicators of the stage boundaries. This objective model for the life cycle of an electropore facilitates comparisons of

bilayer systems of different compositions, subjected to different conditions; and it is our expectation that it will contribute, along with other efforts along these lines (Bockmann et al. 2008), to the development of a coherent mechanism for membrane electroporation that is consistent with molecular and continuum models, with experimental systems of artificial bilayers and with living cell membranes.

Our results show that pore creation and annihilation times are nonlinearly dependent on the porating electric field and that some stages of electroporation are strongly field-dependent while others are insensitive to the magnitude of the field. This MD model of electroporation is at least broadly consistent with the stochastic pore hypothesis for electropermeabilization (Sugar and Neumann 1984; Popescu et al. 1991; Neu and Krassowska 1999; Weaver 2003), and that model may now be enhanced by the incorporation of multiple, field-dependent and field-independent, steps in pore creation and annihilation.

Stages of Electroporation

Pore initiation, the formation of a water column across the membrane interior, is the major field-dependent step in pore creation. Pores initiate more quickly in higher electric fields. This is not surprising in light of previous work showing that the electric field gradient in the bilayer interface region drives water dipoles into the membrane (Tieleman 2004). Pore construction and maturation, the stages following initiation, are not strongly dependent on the magnitude of the porating electric field over the range investigated here, indicating that the reorganization and inward migration of lipid head groups during pore formation are driven at least as much by intermolecular forces promoting association with the water in the bilayer interior as by the applied electric field. If the external field is removed immediately after pore initiation, however, pore construction does not proceed, and the bilayer-bridging water column collapses.

Pore annihilation is broadly analogous to pore creation, although it is by no means simply pore creation run in reverse. During destabilization, the first step in annihilation, we observe shrinkage but no other obvious changes in the gross structure of the pore. Water and head group dipoles are relaxing during this phase, and without the electric field there is no energy to maintain the intermolecular arrangements associated with the hydrophilic pore (Ziegler and Vernier 2008). Although more data are needed, our results show that the pore destabilization time (and the overall pore annihilation time) decreases slightly at the highest field tested. We hypothesize that these "high-field pores" are less ordered than pores formed at lower fields and, thus, easier to disassemble since the water and phospholipid head group components will not have settled so far into local energy minima. Still, this correlation is small, and stochastic effects may be dominating our results. Additionally, the structure of the pore, independent of how it was created, may be the dependent variable which affects pore annihilation; and in this case we are observing the effects of modulating the pore-initiating electric field on the pore structure itself.

A measure of the stability of a pore, once formed, may be taken from the observation that in these simulations pore deconstruction on average takes about 75 times longer than pore construction. Pore deconstruction and dissolution (like construction and maturation) show little field dependence. Overall, pore annihilation appears to consist of both deterministic and stochastic elements, with the primarily stochastic stages accounting for most of the annihilation time.

DOPC Versus POPC

Pore creation times for the POPC and DOPC systems reported here are similar when simulations with similar internal electric fields are compared. Because electropore formation involves primarily a reorganization of water and head groups at the interface, it is not surprising that the saturation or unsaturation of the second fatty acid residue does not strongly affect the pore creation time of a homogeneous bilayer, despite other differences in physical properties (Tieleman et al. 1997). It may be, however, that in more complex systems containing multiple phospholipids and other components like cholesterol (Kucerka et al. 2009), sphingolipids and cytoskeletal attachments (Rols and Teissie 1992), the extent of saturation in the phospholipids may be significant.

Pore creation times for POPC and DOPC are inversely dependent on the membrane internal electric field, and regardless of the lipid type, systems with similar internal electric fields have similar pore creation times, suggesting that it may be useful in MD studies to regard the electric field differential across the membrane interface as a fundamental determinant of the poration process. We note that the y-intercept in Fig. 4 can be interpreted as the projected pore creation time when the electric field is zero, a value which is also represented in continuum models for pore creation and which is related to the basal permeability of artificial lipid bilayers and cell membranes. This kind of intersection may contribute to the bridging of gaps between atomically detailed simulations, mathematical and physical models and experiment.

Deficiencies in the Electropore Life Cycle Scheme

The electropore life cycle model presented here has at least three significant deficiencies. First, although our definition

of a "mature" pore is convenient and not altogether arbitrary, it is not based on the physical properties of pores in real systems because these are not known at this time at the molecular level. We would like to define a "mature" pore that corresponds to the quasi-stable structures that form in artificial lipid bilayers and living cell membranes exposed to electric fields, but at present no such definition exists (Teissie et al. 2005). We hope to investigate this unexplored territory through simulations in which a balance is struck between pore diameter, electrical conductance and applied electric field.

Second, the simulation times are very short, much less than a microsecond. Although this MD regime is well suited for comparisons to data from experiments using nanosecond pulsed electric fields, it is possible that the much longer rise times, lower fields and longer pulses (microseconds to milliseconds) associated with conventional electroporation technology result in a different energy landscape for pore formation and porated membrane structures that are significantly different from those we observe in the systems reported here. More powerful computing hardware and smarter simulation software combined with well-designed experiments will tell us whether this is so.

Third, an important stage may be missing. It is possible that what we have called pore initiation actually includes two steps, somewhat analogous to the first two steps in pore annihilation. In the first of these two steps, the true initiating step, thermal jostling of water dipoles and head groups in the interface, driven more along one path than another by the applied electric field and the membrane internal electric field, results in the pre-pore bumps described previously (Ziegler and Vernier 2008). A hypothetical structure which we have not yet identified develops in some small percentage of these bumps, either as the bump is formed or as a consequence of the continued interaction of the bump with the electric field. This structure represents the low energy path to formation of the membrane-spanning water column, a clear signature of commitment to pore formation. If there is a missing stage, it would represent the conversion of a pre-pore bump to a structure from which water is launched into the membrane interior—a pore pedestal. This pedestal structure, at least the water components of it, may have features in common with the pyramidal or conical features associated with the electric field-enhanced evaporation of water (Okuno et al. 2009).

It is also possible that the missing stage is not really a separate step at all but, rather, a statistical selection of a pore-promoting structure from all of the randomly formed pre-pore bump configurations. Our efforts to identify a signature for this putative pore pedestal have been unsuccessful to date (Ziegler and Vernier 2008). It has been proposed that lipid protrusions, dragging water into the bilayer interior and promoting a dielectric avalanche, are the primary actors in electropore formation (Bockmann et al. 2008). However, we observe many lipid protrusions (bumps of water and lipid) in our simulations. Only very few of them result in pore formation, and we have been unable to detect any head group dipole configuration or density fluctuation associated with the lipids in these bumps that correlates with pore formation (Vernier and Ziegler 2007). Although cooperative associations of water and lipid head groups undoubtedly play an important role in pore formation, the fact that we observe electroporation in simulations of phospholipid bilayers with chargeless head groups (Vernier and Ziegler 2007) and even in octane systems (Tieleman et al. 2003) leads us to believe that rather than look at lipids we should *cherchez l'eau*.

Acknowledgements We thank D. Peter Tieleman for stimulating discussions and insightful input. Computing resources were provided by the USC Center for High Performance Computing and Communications. This work was made possible in part by the Air Force Office of Scientific Research and by MOSIS, Information Sciences Institute, Viterbi School of Engineering, University of Southern California.

References

Abidor IG, Arakelyan VB, Chernomordik LV et al (1979) Electric breakdown of bilayer lipid-membranes. 1. Main experimental facts and their qualitative discussion. Bioelectrochem Bioenerg 6:37–52

Benz R, Zimmermann U (1980) Pulse-length dependence of the electrical breakdown in lipid bilayer-membranes. Biochim Biophys Acta 597:637–642

Berendsen HJC, Postma JPM, van Gunsteren WF, Hermans J (1981) Interaction models for water in relation to protein hydration. In: Pullman B (ed) Intermolecular forces. Reidel, Dordrecht, the Netherlands, pp 331–342

Berendsen HJC, Postma JPM, Vangunsteren WF et al (1984) Molecular-dynamics with coupling to an external bath. J Chem Phys 81:3684–3690

Berger O, Edholm O, Jahnig F (1997) Molecular dynamics simulations of a fluid bilayer of dipalmitoylphosphatidylcholine at full hydration, constant pressure, and constant temperature. Biophys J 72:2002–2013

Bockmann RA, de Groot BL, Kakorin S et al (2008) Kinetics, statistics, and energetics of lipid membrane electroporation studied by molecular dynamics simulations. Biophys J 95:1837–1850

Essmann U, Perera L, Berkowitz ML et al (1995) A smooth particle mesh Ewald method. J Chem Phys 103:8577–8593

Glaser RW, Leikin SL, Chernomordik LV et al (1988) Reversible electrical breakdown of lipid bilayers—formation and evolution of pores. Biochim Biophys Acta 940:275–287

Gurtovenko AA, Vattulainen I (2009) Calculation of the electrostatic potential of lipid bilayers from molecular dynamics simulations: methodological issues. J Chem Phys 130:215107

Hamilton WA, Sale AJH (1967) Effects of high electric fields on microorganisms. 2. Mechanism of action of lethal effect. Biochim Biophys Acta 148:789–800

Hess B, Bekker H, Berendsen HJC et al (1997) LINCS: a linear constraint solver for molecular simulations. J Comput Chem 18:1463–1472

Humphrey W, Dalke A, Schulten K (1996) VMD: visual molecular dynamics. J Mol Graph 14:33–38

Kucerka N, Marquardt D, Harroun TA et al (2009) The functional significance of lipid diversity: orientation of cholesterol in bilayers is determined by lipid species. J Am Chem Soc 131:16358

Leontiadou H, Mark AE, Marrink SJ (2004) Molecular dynamics simulations of hydrophilic pores in lipid bilayers. Biophys J 86:2156–2164

Mir LM, Bureau MF, Gehl J et al (1999) High-efficiency gene transfer into skeletal muscle mediated by electric pulses. Proc Natl Acad Sci USA 96:4262–4267

Miyamoto S, Kollman PA (1992) Settle—an analytical version of the shake and rattle algorithm for rigid water models. J Comput Chem 13:952–962

Neu JC, Krassowska W (1999) Asymptotic model of electroporation. Phys Rev E 59:3471–3482

Neumann E, Schaeferridder M, Wang Y et al (1982) Gene-transfer into mouse lyoma cells by electroporation in high electric-fields. EMBO J 1:841–845

Okuno Y, Minagawa M, Matsumoto H et al (2009) Simulation study on the influence of an electric field on water evaporation. J Mol Struct 904:83–90

Popescu D, Rucareanu C, Victor G (1991) A model for the appearance of statistical pores in membranes due to self oscillations. Bioelectrochem Bioenerg 25:91–103

Rols MP, Teissie J (1990) Electropermeabilization of mammalian cells—quantitative analysis of the phenomenon. Biophys J 58:1089–1098

Rols MP, Teissie J (1992) Experimental evidence for the involvement of the cytoskeleton in mammalian cell electropermeabilization. Biochim Biophys Acta 1111:45–50

Rols MP, Coulet D, Teissie J (1992) Highly efficient transfection of mammalian cells by electric-field pulses—application to large volumes of cell culture by using a flow system. Eur J Biochem 206:115–121

Sengupta D, Leontiadou H, Mark AE et al (2008) Toroidal pores formed by antimicrobial peptides show significant disorder. Biochim Biophys Acta Biomembr 1778:2308–2317

Sugar IP, Neumann E (1984) Stochastic model for electric field-induced membrane pores. Electroporation Biophys Chem 19:211–225

Tarek M (2005) Membrane electroporation: a molecular dynamics simulation. Biophys J 88:4045–4053

Teissie J, Golzio M, Rols MP (2005) Mechanisms of cell membrane electropermeabilization: a minireview of our present (lack of?) knowledge. Biochim Biophys Acta 1724:270–280

Tieleman DP (2004) The molecular basis of electroporation. BMC Biochem 5:10

Tieleman DP, Marrink SJ, Berendsen HJC (1997) A computer perspective of membranes: molecular dynamics studies of lipid bilayer systems. Biochim Biophys Acta Biomembr 1331:235–270

Tieleman DP, Leontiadou H, Mark AE et al (2003) Simulation of pore formation in lipid bilayers by mechanical stress and electric fields. J Am Chem Soc 125:6382–6383

Van der Spoel D, Lindahl E, Hess B et al (2005) GROMACS: fast, flexible, and free. J Comput Chem 26:1701–1718

Vernier PT, Ziegler MJ (2007) Nanosecond field alignment of head group and water dipoles in electroporating phospholipid bilayers. J Phys Chem B 111:12993–12996

Weaver JC (2003) Electroporation of biological membranes from multicellular to nano scales. IEEE Trans Dielectr Electr Insul 10:754–768

Weaver JC, Chizmadzhev YA (1996) Theory of electroporation: a review. Bioelectrochem Bioenerg 41:135–160

Weaver JC, Mintzer RA (1981) Decreased bilayer stability due to transmembrane potentials. Phys Lett A 86:57–59

Ziegler MJ, Vernier PT (2008) Interface water dynamics and porating electric fields for phospholipid bilayers. J Phys Chem B 112:13588–13596